Improving Lidar Turbulence Estimates for Wind Energy

Preprint

Jennifer Newman, Andrew Clifton,
and Matthew Churchfield
National Renewable Energy Laboratory

Petra Klein
University of Oklahoma

To be presented at the Science of Making Torque from Wind (TORQUE 2016)
Munich, Germany
October 5–7, 2016

NREL is a national laboratory of the U.S. Department of Energy
Office of Energy Efficiency & Renewable Energy
Operated by the Alliance for Sustainable Energy, LLC

This report is available at no cost from the National Renewable Energy Laboratory (NREL) at www.nrel.gov/publications.

Conference Paper
NREL/CP-5000-66994
October 2016

Contract No. DE-AC36-08GO28308

NOTICE

This report is available at no cost from the National Renewable Energy Laboratory (NREL) at www.nrel.gov/publications.

Available electronically at SciTech Connect http:/www.osti.gov/scitech

Available for a processing fee to U.S. Department of Energy and its contractors, in paper, from:

U.S. Department of Energy
Office of Scientific and Technical Information
P.O. Box 62
Oak Ridge, TN 37831-0062
OSTI http://www.osti.gov
Phone: 865.576.8401
Fax: 865.576.5728
Email: reports@osti.gov

Available for sale to the public, in paper, from:

U.S. Department of Commerce
National Technical Information Service
5301 Shawnee Road
Alexandria, VA 22312
NTIS http://www.ntis.gov
Phone: 800.553.6847 or 703.605.6000
Fax: 703.605.6900
Email: orders@ntis.gov

Cover Photos by Dennis Schroeder: (left to right) NREL 26173, NREL 18302, NREL 19758, NREL 29642, NREL 19795.

NREL prints on paper that contains recycled content.

Improving lidar turbulence estimates for wind energy

J F Newman[1], A Clifton[1], M J Churchfield[1] and P Klein[2]

[1] National Renewable Energy Laboratory, Golden, CO, USA
[2] School of Meteorology, University of Oklahoma, Norman, OK, USA

E-mail: Jennifer.Newman@nrel.gov

Abstract. Remote sensing devices (e.g., lidars) are quickly becoming a cost-effective and reliable alternative to meteorological towers for wind energy applications. Although lidars can measure mean wind speeds accurately, these devices measure different values of turbulence intensity (TI) than an instrument on a tower. In response to these issues, a lidar TI error reduction model was recently developed for commercially available lidars. The TI error model first applies physics-based corrections to the lidar measurements, then uses machine-learning techniques to further reduce errors in lidar TI estimates. The model was tested at two sites in the Southern Plains where vertically profiling lidars were collocated with meteorological towers. Results indicate that the model works well under stable conditions but cannot fully mitigate the effects of variance contamination under unstable conditions. To understand how variance contamination affects lidar TI estimates, a new set of equations was derived in previous work to characterize the actual variance measured by a lidar. Terms in these equations were quantified using a lidar simulator and modeled wind field, and the new equations were then implemented into the TI error model.

1. Introduction

Procedures such as wind resource assessment and turbine site suitability require measurements of the mean wind speed and turbulence intensity (TI) at the turbine hub height. Traditionally, these measurements have been collected by cup anemometers on tall meteorological (met) towers. However, as modern turbine hub heights increase, it becomes more difficult and costly to install met towers to reach hub height; in response, remote sensing devices (e.g., lidars, or light detection and ranging devices) have recently emerged as alternatives to met towers. Although lidars have several advantages over met towers, measurement methods used by lidars are fundamentally different than those used by a cup or sonic anemometer. Anemometers provide an estimate of the wind speed at a small volume in space whereas lidars provide an average across a probe volume; this probe volume varies in length in the along-beam direction depending on the lidar used and is 20 m long for the WINDCUBE v2 lidar employed in this work. In addition, lidars only provide an estimate of the line-of-sight velocity and must point the lidar beam toward different azimuth angles around a scanning circle to derive the full three-dimensional wind field. This scanning circle, which has a diameter of approximately 100 m for a commercial lidar at a measurement height of 100 m, introduces a phenomenon known as variance contamination [1]. Finally, instrument noise from the lidar can increase the variance estimated from the lidar measurements (for example, see [2]). All three of these factors—volume averaging, variance contamination, and instrument noise—have negligible effects on the mean wind speed estimated from the lidar but have profound effects on the lidar-estimated turbulence. Lidars must be

able to measure turbulence accurately to be viewed as a viable alternative to met towers in the wind energy industry. Thus, there is clearly a need for more accurate lidar-based turbulence estimates, particularly for commercial lidars.

In response to this need for more accurate lidar turbulence estimates, an algorithm was recently developed to reduce error in turbulence measurements from commercial lidars. The Lidar Turbulence Error Reduction Algorithm (L-TERRA) incorporates physics-based corrections, such as a spike filter and spectral corrections, in addition to machine-learning methods to improve lidar turbulence estimates. In this paper, the development and testing of L-TERRA are discussed and results from two sites in the Southern Plains are shown. A lidar simulator is used to improve the variance contamination corrections in L-TERRA and future applications of the lidar simulator in improving lidar turbulence estimates are discussed.

2. Background

2.1. Lidar technology

Lidars emit light waves into the atmosphere, which are then scattered by aerosol particles. A small portion of the scattered radiation returns to the lidar, and the Doppler shift of the returned radiation is used to estimate the velocity in the line-of-sight of the lidar. In the case of a pulsed Doppler lidar, the returned signal time series is split into blocks that correspond to range gates [3].

L-TERRA was initially developed for the WINDCUBE v2 lidar (Leosphere, Orsay, France), hereafter referred to as "WC," a commercially available, pulsed Doppler lidar that is commonly used in the wind energy industry. The WC uses a Doppler-beam swinging (DBS) [4] technique to estimate the three-dimensional wind profile, wherein the lidar beam is pointed in the north, east, south, and west directions and geometrical relations are used to estimate the u, v, and w wind components. The WINDCUBE v2 model, which was used in this work, includes a vertically pointing beam position to obtain a direct measurement of the vertical velocity. The WC accumulates measurements at each scanning location for 1 s, and a full scan takes approximately 4 s. However, the device's software updates the velocity vector every time the beam moves to a new location, such that the output data stream of velocity is available at 1 Hz.

2.2. Sources of lidar turbulence error

Three primary factors impact the accuracy of lidar turbulence estimates: instrument noise, volume averaging, and variance contamination. The first two factors are inherent to remote sensing technology and impact any type of lidar regardless of the scanning technique used. Instrument noise results from factors such as the limited amount of scatterers in the lidar probe volume (for example, see [2]) and spontaneous laser emissions [5]. Volume averaging occurs because the lidar must receive backscattered radiation from a volume of air, rather than a point, to obtain a sufficient amount of data for estimation of the radial wind speed. For the WC lidar used in this work, the sample volume is 20 m in length and negligibly small in the cross-beam direction [6]. Thus, the lidar-measured wind speed at a height of 100 m is actually a weighted average of all the aerosol particle velocities between 90 and 110 m. The probe volume acts as a low-pass filter, as high-frequency motion that occurs on spatial scales smaller than the probe volume of the lidar cannot be resolved.

The third factor, variance contamination, is caused by the scanning strategy used by the lidar. When velocity data from different parts of the lidar scanning circle are combined to estimate the raw wind speed components, it is assumed that the instantaneous wind field is uniform across the scanning circle. However, this assumption is not true in turbulent flow, and changes in the wind field across the lidar scanning circle introduce additional variance components into the calculation of the u, v, and w variance (for example, see [1] and [7]).

Various methods have been proposed for reducing error in lidar turbulence estimates, including fitting a turbulence model (for example, see [1]), using a new six-beam scanning technique [8], and employing multiple scanning lidars (for example, see [9]). Although these techniques improved lidar turbulence estimates in a research context, they require the use of sonic anemometer data and/or expensive scanning lidars, which are not often available outside a research setting. Thus, this work focuses on improving turbulence estimates from vertically profiling lidars that are commonly used in the wind energy industry. Even though these lidars are not as powerful or versatile as scanning lidars, vertically profiling lidars provide a wealth of valuable information that can be used to improve turbulence estimates.

3. Approach and methods

3.1. L-TERRA

A simplified flowchart depicting the use of L-TERRA to improve lidar turbulence estimates is shown in Figure 1. The physics-based corrections are comprised of different methods for mitigating errors from instrument noise, volume averaging, and variance contamination. The initial estimate of the corrected TI from the physics-based corrections is then used as an input to a machine-learning model, in addition to other lidar-measured parameters. Methods used in L-TERRA are summarized briefly here and discussed in more detail in [10].

3.1.1. Instrument noise To reduce instrument noise, a basic spike filter was evaluated in L-TERRA, in addition to autocovariance and spectral methods discussed by [2].

3.1.2. Volume averaging Structure functions and spectral extrapolation were evaluated in L-TERRA as potential methods to reduce the effects of volume averaging. Values of the structure function at different separation distances can be calculated from lidar data. A modeled form of the structure function that depends on mean wind speed and variance can then be used to estimate turbulence parameters that are unaffected by volume averaging (for example, see [11]). Another method is to fit a model to the lidar velocity spectrum and extrapolate the modeled spectrum out to higher frequencies (for example, see [12]).

3.1.3. Variance contamination The six-beam technique [8] was adapted for use by the five WC lidar beams, as described in [7], to reduce variance contamination. In addition, Taylor's frozen turbulence hypothesis was used to estimate the change in vertical velocity across the lidar scanning circle and remove the effect of this change on the horizontal variance components [13].

3.1.4. Machine learning The trained machine-learning model in L-TERRA relates lidar-measured parameters, such as the shear exponent and signal-to-noise ratio (SNR), to the difference between the initially corrected lidar TI and the met tower TI to produce the final estimate of the corrected lidar TI. Machine-learning methods evaluated in L-TERRA were random forests, multivariate-adaptive regression splines, and support vector regression.

In [10], all possible combinations of the different error mitigation methods in L-TERRA were evaluated to determine the optimal model chain for each field measurement site. Corrected TI estimates shown in this work are results from these optimal configurations of L-TERRA.

3.2. Lidar simulator

When a lidar is deployed near a met tower, errors in mean wind speed and TI in comparison to the tower instruments can be easily quantified. However, it is not as straightforward to determine why these errors actually occur, as the true flow field measured by the lidar is largely

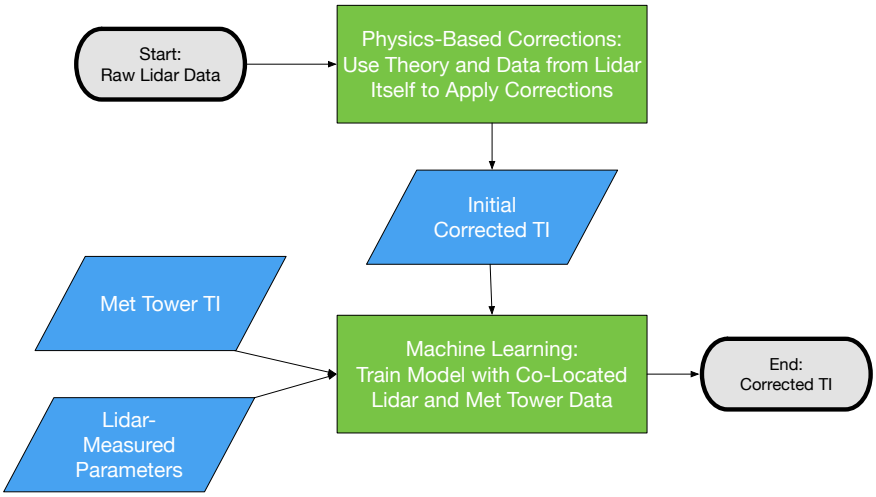

Figure 1. Flowchart depicting the basic structure for correcting TI with L-TERRA.

unknown. With a lidar simulator, a prescribed wind field can be sampled by the simulated lidar and compared to the point measurements from different parts of the scanning circle. In this work, the virtual lidar tool implemented in the National Renewable Energy Laboratory's (NREL's) Simulator fOr Wind Farm Applications (SOWFA) [14] was used to simulate lidar measurement techniques.

SOWFA is an atmospheric large-eddy simulation tool that can model the full atmospheric boundary layer. The virtual lidar tool samples the flow field along specified lines representing lidar beams at a given frequency. The large-eddy simulation flow field is sampled at points along the lines using linear interpolation, which is equal in order of accuracy to the spatial discretization of the solver itself.

For this work, the virtual lidar tool was used to sample inflow to a 32.6-m hub-height turbine at Texas Tech University's Scaled Wind Farm Technology facility under unstable atmospheric conditions. The domain was 4 km by 7 km by 2 km, with the predominant flow direction along the 7-km length of the domain, a spatial resolution of 5 m, a temporal resolution of 1 s, and periodic lateral boundary conditions. The mean wind speed and TI at hub height were 6.5 m s^{-1} and 17.2%, respectively. To achieve unstable convective conditions, a surface temperature flux of 0.1 K m s^{-1} was specified at the lower surface. An initial capping inversion with a strength of 3 K m^{-1} was placed at 1300 m above the surface, and the simulation was advanced for 2 hours before it reached a quasi-equilibrium state.

After reaching equilibrium, samples were extracted from four virtual lidars placed 1 km apart in the turbine inflow region. Simulation data were extracted from four beams spaced 90° apart at an elevation angle of 60° and one vertical beam to mimic the scanning configuration of the WC. A weighting function was applied to the simulated velocity data in postprocessing to simulate volume averaging within each lidar probe volume (for example, see [14]). To the authors' knowledge, there is currently no accepted method for modeling noise in Doppler lidar data, although any such model could be easily implemented into the virtual lidar tool in postprocessing. The current version of the virtual lidar tool does not simulate instrument noise.

4. L-TERRA results

4.1. Sites

Three sites were used to train and test the initial version of L-TERRA: the Atmospheric Radiation Measurement (ARM) site in northern Oklahoma, the Boulder Atmospheric

Observatory (BAO) in Erie, Colorado, and an operational wind farm in the Southern Great Plains region of the United States. Because of a nondisclosure agreement with the wind farm, its exact location cannot be disclosed. Only data from the ARM site and wind farm are shown in this work, as lidar data availability was low at the BAO due to a low aerosol count.

The ARM site is a field measurement site operated by the U.S. Department of Energy that contains a variety of in-situ and remote sensing instruments [15]. From November 2012 to July 2013, a WC lidar was deployed 100 m northeast of a 60-m tower at the ARM site with Gill Windmaster Pro 3-D sonic anemometers mounted at 25 and 60 m above ground level (AGL). The WC was then deployed at the operational wind farm from November 2013 to January 2014 and again from May to July 2014. While at the wind farm, the WC was located in the same enclosure as a met tower containing standard wind energy instrumentation. The tower had a lattice structure and the WC was positioned such that none of the beam positions were blocked by the tower. The closest turbine was approximately 240 m from the tower enclosure, and only measurements from nonwaked wind directions were used in this work.

4.2. Initial lidar TI

Examples of sonic and cup anemometer versus lidar TI are shown in Figure 2 for the Southern Plains sites. Stability was stratified according to the shear parameter, α, with thresholds given in Table 1. The shear parameter was calculated using WC data from 40 to 200 m. Negative shear parameters corresponded to cases with lower wind speeds at 200 m than at 40 m and following standard wind engineering practices, these cases were classified as strongly unstable.

The main sources of TI error are largely evident in Figure 2: volume averaging causes the lidar to underestimate TI under stable conditions, when scales of turbulent motion are small, whereas variance contamination causes the lidar to overestimate TI under unstable conditions, when scales of turbulence are larger and volume averaging is not as prevalent.

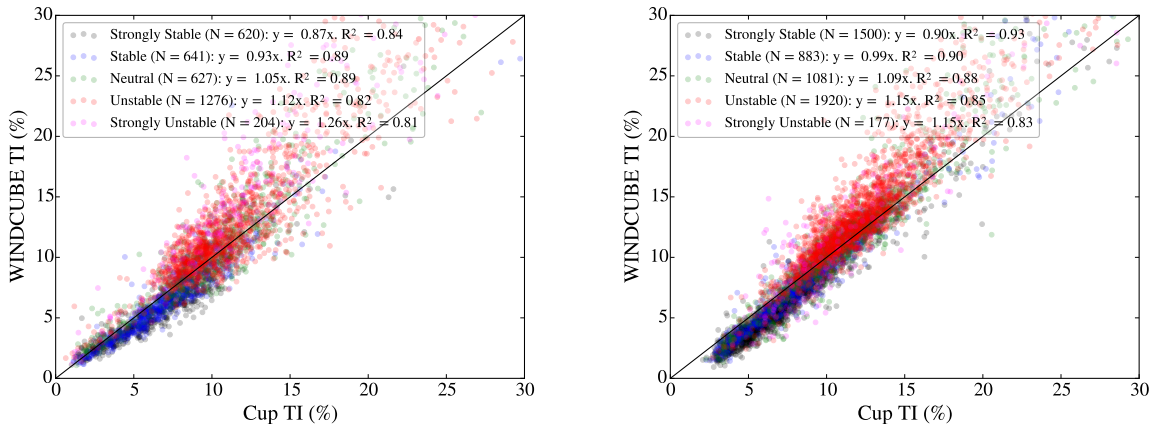

(a) ARM Site **(b)** Wind Farm

Figure 2. Lidar versus tower TI for the: a) ARM site at 60 m AGL and b) wind farm at 80 m AGL. Regression line equations and R^2 values are given in figure legends.

4.3. Corrected lidar TI

Figure 3 shows the lidar TI after L-TERRA has been applied to data from both sites. Although the regression line slopes for all the stability classes are now closer to 1 in comparison to the original TI, there are still many large discrepancies between the met tower and corrected lidar

Table 1. Stability classifications used in this work.

Stability Classification	Shear Parameter Range
Strongly stable	$\alpha \geq 0.3$
Stable	$0.2 \leq \alpha < 0.3$
Neutral	$0.1 \leq \alpha < 0.2$
Unstable	$0 \leq \alpha < 0.1$
Strongly unstable	$\alpha < 0$

TI. To identify conditions under which L-TERRA performance is suboptimal, histograms of TI, mean wind speed, and the shear parameter were examined for periods in which the difference between the corrected lidar TI and met tower TI was still greater than 3%. At the ARM site, these periods comprised 5.2% of the testing data set. Before L-TERRA was applied, 12.2% of the lidar TI values in the testing data set had an error of more than 3%.

Histograms from the ARM site are shown in Figure 4. Large differences between the corrected lidar TI and sonic TI tend to occur when the lidar measures high TI values, low mean wind speed values, and low shear parameter values in comparison to the testing data set as a whole. These trends typically correspond to unstable atmospheric conditions, suggesting that in their current form, neither the physics-based corrections nor the machine-learning techniques in L-TERRA can adequately mitigate the effects of variance contamination. The initial version of the variance contamination module utilizes Taylor's frozen turbulence hypothesis, which is less valid for lower wind speeds when turbulent eddies are more likely to evolve as they move across the lidar scanning circle. Thus, it is not surprising that large TI errors remain for low wind speed conditions.

It is also likely that the machine-learning portion of L-TERRA did not have an adequate amount of training data under these high-TI, low wind speed conditions. The histograms shown in Figure 4 indicate that outlier conditions correspond to the tail of the TI training set distribution and the far left ends of the mean wind speed and shear distributions. Thus, the conditions under which L-TERRA performed most poorly also correspond to conditions in which the machine-learning model was not supplied with a large amount of training data and is not expected to perform as well. This highlights the need for a large training data set for L-TERRA that includes a wide range of conditions.

5. New method for reducing variance contamination

5.1. Theoretical background

A series of equations was developed in [7] to relate the variance measured by a lidar with a DBS technique to the true value of the variance through the use of autocorrelation functions (ACFs). This series of equations is essentially a simplified version of the results presented in [1], in which a model of the spectral velocity tensor is convolved with a volume-averaging function to estimate the variance that would be measured by a lidar. This modeling approach typically requires fitting parameters to sonic anemometer data and is technically only valid under neutral conditions. In contrast, the technique presented in this work does not require the fitting of a model and is much simpler to implement. A brief overview of the development of this technique is given here.

The radial velocity, v_r, measured with the DBS technique at different beam positions, can be described by the following equations:

$$v_{r1} = v_1 \cos\phi + w_1 \sin\phi \tag{1}$$

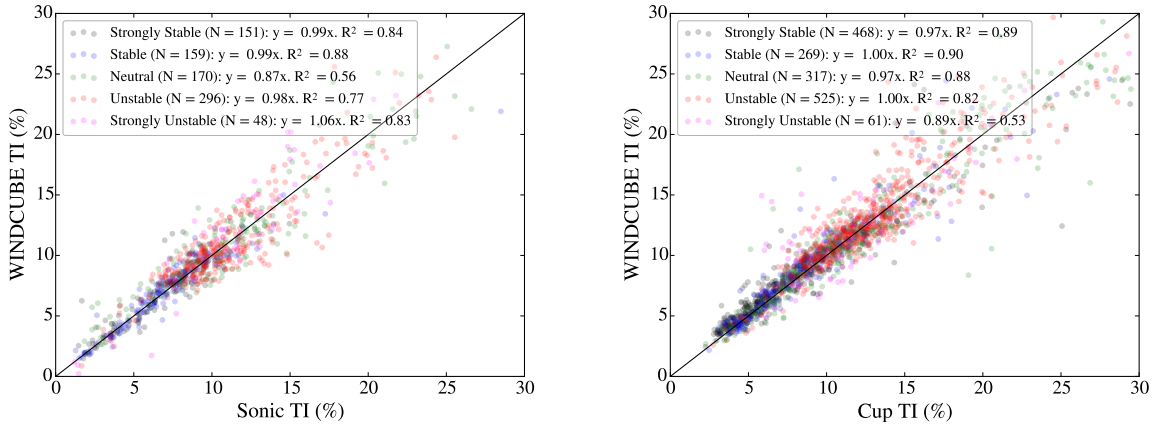

(a) ARM Site **(b)** Wind Farm

Figure 3. Corrected lidar versus tower TI for the: a) ARM site at 60 m AGL and b) wind farm at 80 m AGL. Regression line equations and R^2 values are given in figure legends. Only 25% of the TI data are shown, as the remaining 75% of the data were used to train the machine-learning module in L-TERRA.

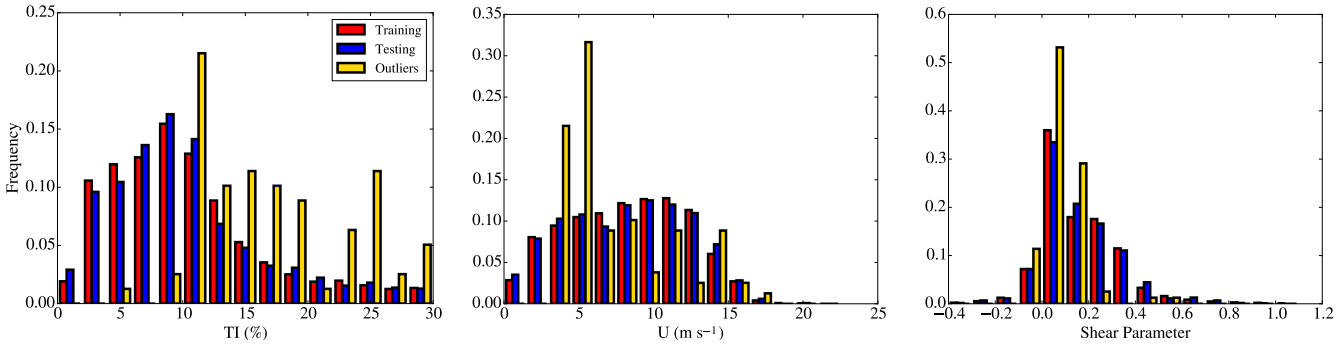

(a) **(b)** **(c)**

Figure 4. Histograms of a) TI, b) mean wind speed, U, and c) shear parameter from the ARM site training and testing data sets. Yellow bars indicate histograms for cases in which $|TI_{lidar,corrected} - TI_{sonic}| > 3\%$ after L-TERRA has been applied to the testing data set.

$$v_{r2} = u_2 \cos\phi + w_2 \sin\phi \tag{2}$$

$$v_{r3} = -v_3 \cos\phi + w_3 \sin\phi \tag{3}$$

$$v_{r4} = -u_4 \cos\phi + w_4 \sin\phi \tag{4}$$

where u is the east-west wind component, v is the north-south wind component, w is the vertical wind component, ϕ is the elevation angle of the lidar beam, and subscripts $1, 2, 3$, and 4 correspond to the north, east, south, and west directions, respectively. For the DBS technique,

it is assumed that $v_1 = v_3 = v$, $u_2 = u_4 = u$, and $w_1 = w_2 = w_3 = w_4 = w$, which gives the following set of equations for determining values of the u, v, and w wind components [6]:

$$u = \frac{v_{r2} - v_{r4}}{2\cos\phi} \tag{5}$$

$$v = \frac{v_{r1} - v_{r3}}{2\cos\phi} \tag{6}$$

$$w = \frac{v_{r1} + v_{r2} + v_{r3} + v_{r4}}{2\sin\phi} \tag{7}$$

If the lidar model includes a fifth, vertically pointing beam, as does the model used in this work, w can also be approximated as $w = v_{r5}$. The time series of u, v, and w can then be used to calculate the variance components and TI. However, if the instantaneous velocity components change across the scanning circle, as is often the case in turbulent flow, then additional variance components will contaminate the true value of the variance. It was shown in [7] that in this case, the true u and v variance values can be expressed by the following equations:

$$\overline{u'^2} = \frac{2}{1+\rho_u}\overline{u'^2_{DBS}} - \frac{(1-\rho_w)\sin^2\phi}{(1+\rho_u)\cos^2\phi}\overline{w'^2} \tag{8}$$

$$\overline{v'^2} = \frac{2}{1+\rho_v}\overline{v'^2_{DBS}} - \frac{(1-\rho_w)\sin^2\phi}{(1+\rho_v)\cos^2\phi}\overline{w'^2} \tag{9}$$

where the subscript DBS refers to estimates from the lidar, ρ_u, ρ_v, and ρ_w are autocorrelation functions (ACFs) that describe the autocorrelation values of the u, v, and w velocity components, respectively, measured at different positions along the scanning circle, and $\overline{w'^2}$ is the value of the vertical variance measured by the WC's vertical beam. If the instantaneous wind field is assumed to be uniform across the lidar scanning circle, as it is with the DBS technique, then $\rho_u = \rho_v = \rho_w = 1$ and the horizontal variance values are simply calculated by taking the variance of Equations 5 and 6. However, when the velocity components decorrelate across the scanning circle, which is often true in turbulent flow, then the ACFs are not equal to 1 and the true value of the variance is contaminated by additional components (Equations 8 and 9). In the following section, characteristic values of the ACFs are estimated using the virtual lidar tool and the ACF technique is implemented in L-TERRA.

5.2. Application to lidar data

In [7], values of the ACFs were estimated from 100-m sonic anemometer data from opposite booms at the BAO. Mean values of ρ_u, ρ_v, and ρ_w estimated under unstable conditions were 0.96, 0.81, and 0.66, respectively, and 0.95, 0.71, and 0.69 under stable conditions. Newman et al. [7] also estimated values of the ACFs by obtaining least-squares solutions to Equations 8 and 9 for WC and sonic data at the BAO, finding similar values of ρ_u and ρ_v to those estimated from the sonic anemometers and values of 0.29 and 0.13 for ρ_w under unstable and stable conditions, respectively. Although using these ACF values did reduce variance contamination somewhat in the WC data, they do not represent the actual decorrelation that occurs between WC beams.

In this work, the virtual lidar tool was used to estimate realistic values of the ACFs for the distance spanned by the lidar scanning circle and the time it takes the lidar beam to move from one side of the scanning circle to the other. For these initial estimates, only data under unstable conditions were used in the simulation, as variance contamination is most prominent under unstable conditions when compensation by volume averaging is small [1].

Values of the ACFs for u, v, and w are shown in Figure 5 as a function of height from 50 to 150 m. These ACF values describe the correlation of the u, v, and w wind speeds for a time

lag of 2 s (i.e., the time it takes the WC beam to move from one side of the scanning circle to the other) and for two different spatial separation distances: the distance corresponding to the lidar scanning circle diameter at each height (blue lines) and the distance corresponding to the lidar scanning circle diameter at a height of 100 m (red lines). Plotting the ACFs for a constant separation distance allows for examination of the change in ACFs with height without the influence of the increasing scanning circle diameter.

Mean values of ρ_u that correspond to the scanning circle diameter at each height are approximately 0.55 at 50 m and gradually decrease to 0.4 at a height of 150 m (Figure 5a). Mean values of ρ_v are just under 0.5 at 50 m and similar to ρ_u, decrease with height, reaching a value of approximately 0.37 at 150 m (Figure 5b). However, values of ρ_u and ρ_v that correspond to a constant distance do not change significantly with height. Scales of horizontal turbulence are not expected to change drastically with height in the simulations, as turbulent length scales for u and v tend to scale with the boundary layer height in the convective boundary layer (CBL) [16]. Thus, the increasing diameter of the lidar scanning circle is likely primarily responsible for the decrease in horizontal ACF values with height when a spatial separation corresponding to the scanning circle diameter is used.

The mean value of ρ_w is approximately 0.16 at 50 m for a separation distance corresponding to the changing scanning circle diameter, and mean values increase with height up to about 100 m when the mean value of ρ_w stays at approximately 0.19 between 100 and 150 m (Figure 5c). In the CBL, horizontal fluctuations in w are dominated by updrafts and downdrafts associated with turbulent eddies. These thermal plumes typically merge into larger plumes higher in the CBL (for example, see [17]), causing horizontal fluctuations in w to occur on larger spatial scales. Thus, in contrast to u and v, the horizontal length scale of w fluctuations increases with height. When a constant separation distance is used, values of ρ_w increase more rapidly with height (Figure 5c).

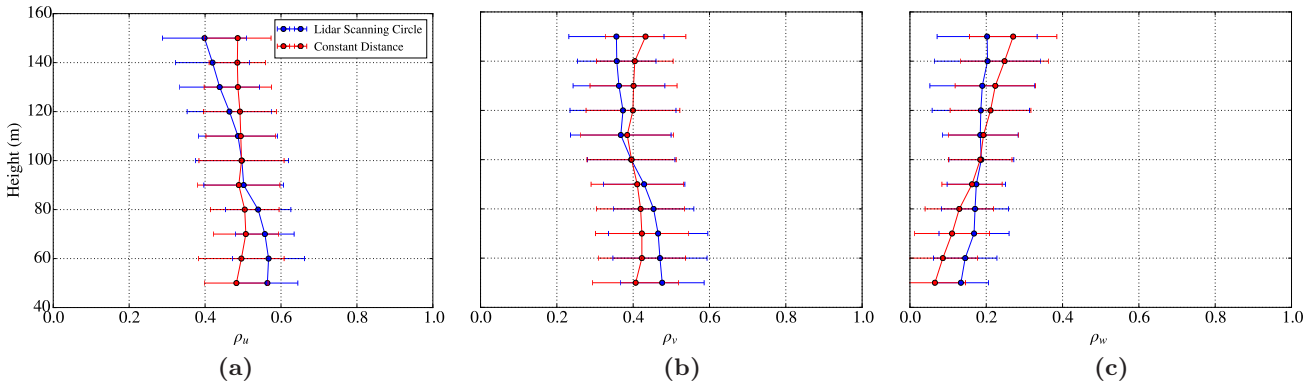

Figure 5. Profiles of the ACF functions for a) u, b) v, and c) w derived from the lidar simulator as a function of height. Circles indicate mean values from twelve 10-min. periods and error bars indicate standard deviation.

Equations 8 and 9 were then used with mean values of the ACFs at a height of 60 m to reduce variance contamination in the ARM site data. As characteristic ACF values were only determined for unstable conditions, this new variance contamination method was only applied to TI estimates under unstable conditions. For TI estimates under neutral and stable conditions, the method involving Taylor's frozen turbulence hypothesis was used to reduce variance contamination [13]. Results from the application of the ACF technique in L-TERRA are shown in Figure 6 for the ARM site.

Incorporating the ACF correction into L-TERRA improved some lidar TI estimates, with regression line slopes increasing from 0.99 to 1.00 under strongly stable conditions and from 0.87 to 0.89 under neutral conditions. The ACF correction had the largest impact on strongly unstable TI estimates, with the regression line slope decreasing from 1.06 to 0.98. However, when the ACF correction was applied, scatter increased significantly for unstable and strongly unstable TI estimates, as evidenced by lower R^2 values in comparison to the original implementation of L-TERRA (Figures 3a, 6). The scatter is likely related to the large spread of ACF values at each height (Figure 5); for example, although the mean 60-m ρ_u value of 0.567 was used in L-TERRA, values of ρ_u at 60 m in the simulator ranged from 0.367 to 0.732. These ACF values represent values from three 10-min. periods at four different locations in simulated flow, suggesting that values of the ACFs can change significantly from one 10-min. period to the next and from one location to another. In addition, values of the ACFs change with both height and scanning circle diameter, making it difficult to apply the ACF correction to lidars with different scanning configurations. These findings highlight the importance of incorporating current flow characteristics into TI corrections, rather than using climatological values of correction factors. Even in the limited data set used in this work, values of the ACFs appear to change significantly depending on the precise atmospheric conditions experienced during each 10-min. period and the separation distance corresponding to the lidar scanning circle diameter at each height.

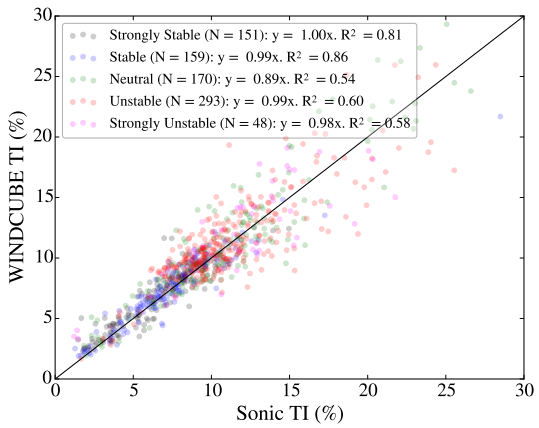

Figure 6. Corrected lidar versus tower TI for the ARM site with the ACF correction used in the variance contamination module of L-TERRA. Only testing data are shown.

6. Discussion and Conclusions

A new model was recently developed to reduce errors in TI measured by Doppler lidars [10]. Initial results shown here indicate that L-TERRA generally reduces TI errors under all stability conditions but does not fully capture TI errors under unstable conditions, likely as a result of variance contamination. Currently, there is no simple method to quantify the effects of variance contamination on lidar TI estimates. Thus, as part of this work, a series of virtual lidars was placed in a modeled wind field to examine the impact of variance contamination on TI estimates and to evaluate equations presented in [7] for reducing variance contamination.

The variance contamination equations contain the parameters ρ_u, ρ_v, and ρ_w, which indicate the degree of correlation between wind components at different sides of the lidar scanning circle. Results from the lidar simulator indicate that these correlations can change significantly from one 10-min. period to the next and for different lidar scanning circle diameters, making it difficult to apply a general variance contamination correction to all lidar TI estimates under unstable

conditions. When mean values of the ACFs were used to reduce variance contamination in L-TERRA, some lidar TI estimates improved, but scatter increased. This result suggests that the variance contamination method must adapt to the differing atmospheric conditions during each 10-min. time period to accurately reduce variance contamination. Future work will involve using available lidar data to quantify the degree of variance contamination during each 10-min. period. By using data from the lidar itself, rather than a generalized equation, variance contamination can be quantified more accurately for different sites and under different kinds of stability conditions. Variance contamination corrections can be tested with the virtual lidar tool to examine the validity of the corrections for different lidar scanning geometries, measurement heights, and atmospheric conditions.

Acknowledgments
The authors would like to thank the scientists and staff members who assisted with the ARM site, BAO, and wind farm deployments. Sebastien Biraud and Marc Fischer supplied sonic anemometer data for the ARM site, and Andreas Muschinski provided sonic anemometer data for the BAO. Sonia Wharton of Lawrence Livermore National Laboratory provided the WINDCUBE lidar used in this work and assisted with field deployments. The ARM Climate Research Facility is a U.S. Department of Energy Office of Science user facility sponsored by the Office of Biological and Environmental Research. This work was supported by the U.S. Department of Energy under Contract No. DE-AC36-08GO28308 with the National Renewable Energy Laboratory. Funding for the work was provided by the DOE Office of Energy Efficiency and Renewable Energy, Wind and Water Power Technologies Office. The U.S. Government retains and the publisher, by accepting the article for publication, acknowledges that the U.S. Government retains a nonexclusive, paid-up, irrevocable, worldwide license to publish or reproduce the published form of this work, or allow others to do so, for U.S. Government purposes.

References

[1] Sathe A, Mann J, Gottschall J and Courtney M S 2011 *J. Atmos. Oceanic Technol.* **28** 853–868

[2] Lenschow D H, Wulfmeyer V and Senff C 2000 *J. Atmos. Oceanic Technol.* **17** 1330–1347

[3] Huffaker R M and Hardesty R M 1996 *Proceedings of the IEEE* **84** 181–204

[4] Strauch R G, Merritt D A, Moran K P, Earnshaw K B and De Kamp D V 1984 *J. Atmos. Oceanic Technol.* **1** 37–49

[5] Chang W S 2005 *Principles of Lasers and Optics* (Cambridge University Press)

[6] Peña A *et al.* 2015 Remote sensing for wind energy Tech. Rep. DTU Wind Energy-E-Report-008 Denmark Technical University

[7] Newman J F, Klein P M, Wharton S, Sathe A, Bonin T A, Chilson P B and Muschinski A 2016 *Atmos. Meas. Tech.* **9** 1993–2013

[8] Sathe A, Mann J, Vasiljevic N and Lea G 2015 *Atmos. Meas. Tech.* **8** 729–740

[9] Fuertes F C, Iungo G V and Porté-Agel F 2014 *J. Atmos. Oceanic Technol.* **31** 1549–1556

[10] Newman J F and Clifton A 2016 *Wind Energ. Sci. Discuss.* In review, doi:10.5194/wes–2016–22

[11] Krishnamurthy R, Calhoun R, Billings B and Doyle J 2011 *Meteorological Applications* **18** 361–371

[12] Hogan R J, Grant A L, Illingworth A J, Pearson G N and O'Connor E J 2009 *Quart. J. Roy. Meteor. Soc.* **135** 635–643

[13] Newman J F 2015 *Optimizing lidar scanning strategies for wind energy turbulence measurements* Ph.D. thesis University of Oklahoma Norman, Oklahoma, USA

[14] Lundquist J K, Churchfield M J, Lee S and Clifton A 2015 *Atmos. Meas. Tech.* **8** 907–920
[15] Mather J H and Voyles J W 2013 *Bull. Amer. Meteor. Soc.* **94** 377–392
[16] Kaimal J C, Wyngaard J C, Haugen D A, Coté O R, Izumi Y, Caughey S J and Readings C J 1976 *J. Atmos. Sci.* **33** 2152–2169
[17] Garratt J 1992 *The Atmospheric Boundary Layer* (Cambridge University Press)